

Common effect of chemical and external pressures on the magnetic properties of $R\text{CoPO}$ ($R = \text{La, Pr, Nd, Sm}$). II.

G. Prando,^{1,*} G. Profeta,² A. Continenza,² R. Khasanov,³ A. Pal,^{4,5} V. P. S. Awana,⁴ B. Büchner,^{1,6} and S. Sanna⁷

¹*Leibniz-Institut für Festkörper- und Werkstofforschung (IFW) Dresden, D-01171 Dresden, Germany*

²*Department of Physical and Chemical Sciences and SPIN-CNR, Università dell'Aquila, I-67100 L'Aquila, Italy*

³*Laboratory for Muon Spin Spectroscopy, Paul Scherrer Institut, CH-5232 Villigen PSI, Switzerland*

⁴*National Physical Laboratory (CSIR), New Delhi 110012, India*

⁵*Department of Physics, Indian Institute of Science, Bangalore 560012, India*

⁶*Institut für Festkörperphysik, Technische Universität Dresden, D-01062 Dresden, Germany*

⁷*Dipartimento di Fisica and Unità CNISM di Pavia, Università di Pavia, I-27100 Pavia, Italy*

(Received 17 June 2015; revised manuscript received 25 September 2015; published 12 October 2015)

We investigate the direct correspondence between Co band ferromagnetism and structural parameters in the pnictide oxides $R\text{CoPO}$ for different rare-earth ions ($R = \text{La, Pr, Nd, Sm}$) by means of muon-spin spectroscopy and *ab initio* calculations, complementing our results published previously [G. Prando *et al.*, Common effect of chemical and external pressures on the magnetic properties of $R\text{CoPO}$ ($R = \text{La, Pr}$), *Phys. Rev. B* **87**, 064401 (2013)]. We find that both the transition temperature to the ferromagnetic phase T_C and the volume of the crystallographic unit cell V are conveniently tuned by the R ionic radius and/or external pressure. We report a linear correlation between T_C and V and our *ab initio* calculations unambiguously demonstrate a full equivalence of chemical and external pressures. As such, we show that R ions influence the ferromagnetic phase only via the induced structural shrinkage without involving any active role from the electronic f degrees of freedom, which are only giving a sizable magnetic contribution at much lower temperatures.

DOI: [10.1103/PhysRevB.92.144414](https://doi.org/10.1103/PhysRevB.92.144414)

PACS number(s): 61.50.Ks, 71.15.Mb, 75.50.Cc, 76.75.+i

I. INTRODUCTION

In the last decade, quaternary $RMXO$ oxides with tetragonal ZrCuSiAs structure (also generally referred to as 1111 compounds) have been extensively investigated on both experimental and theoretical levels. Here, one has an alternating stacked sequence of RO and MX layers along the c axis and, within each layer, R^{3+} (X^{3-}) ions surround O^{2-} (M^{2+}) with a local tetrahedral crystalline arrangement. Depending on the actual choice of the pnictide element X in combination with a transition metal M , different electronic properties can be achieved [1] ranging from high- T_C bulk superconductivity (with T_C values up to 55 K for $M = \text{Fe}$ and $X = \text{As}$) [2–6] to ferromagnetism with rare Kondo features (typically for $M = \text{Ru}$ and $X = \text{P}$) [7,8] or with large – even colossal – magnetoresistance ($M = \text{Co, Mn}$ and $X = \text{As, P}$) [9–15]. However, the complex multiorbital nature of the fermiology [16,17] together with the open issue about the importance of electronic correlations [18,19] makes the overall understanding of these materials still not complete and currently highly debated.

The role of the rare-earth element R is subtle as well. In $R\text{FeAsO}_{1-x}\text{F}_x$ superconductors, R strongly influences the optimal-doping T_C value, which is more than doubled from ~ 25 K in the case of $R = \text{La}$ to ~ 55 K for $R = \text{Sm}$. While it is excluded that this enhancement is associated with $4f$ orbitals and with the localized magnetic moment at the R site [20], no theory can still fully account for the experimental observations. The structural origin (i.e., chemical pressure) seems to be an adequate explanation for the observed effects [21]. However, in this case, it would be

naively expected that also external pressure could enhance T_C in optimally doped systems, which is not the result of experimental observations [22,23]. Chemical dilutions and quenched disorder are expected indeed to crucially drive the superconducting properties as well [24], invalidating this way a full analogy between the effects of external and chemical pressures on T_C [23].

In this respect, the impact of structural effects on the electronic ground state of the system seems to be much easier to control in the absence of intentionally introduced chemical dilutions. This was shown to be the case for undoped $R\text{FeAsO}$ materials, where external pressure (P) weakens the long-range ordered (LRO) antiferromagnetic (AFM) spin-density wave (SDW) phase similarly to what is achieved by means of low values of electron doping [25,26]. At the same time, we have previously reported on a detailed investigation of structural effects in LaCoPO and PrCoPO by means of muon-spin spectroscopy ($\mu^+\text{SR}$) and density-functional theory (DFT) calculations [27], showing that the Co-based ferromagnetic (FM) compounds $R\text{CoPO}$ are an ideal playground to investigate the interplay of chemical and external pressures.

In this paper, we extend our previous investigation to the case of NdCoPO and SmCoPO . As is well known in the literature, the magnetic moment arising from electronic f shells and localized on the Nd^{3+} and Sm^{3+} ions plays a key role in the overall magnetic properties of the compounds [28–30] similarly to the case of their $R\text{CoAsO}$ analogues [12,13,31–37]. In particular, a FM-to-AFM transition is induced within the Co sublattice with decreasing temperature, followed at much lower temperatures by a LRO phase of R magnetic moments [28]. Here, we mainly focus on the high-temperature FM phase within the Co sublattice by showing a strong correlation of the magnetic and structural properties, from a different perspective complementary to our previous approach

*g.prando@ifw-dresden.de

in Ref. [27]. There, we focused on the internal magnetic field at the site of the muon (μ^+), i.e., a quantity proportional to the order parameter of the magnetic phase transition. This quantity is dramatically dependent on the intrinsic technical features of μ^+ SR such as, e.g., the precise implantation site for μ^+ . Being this crystallographic position intrinsically sample dependent even for isostructural materials, it is impossible to draw any quantitative and comprehensive picture about a family of different compounds by only considering this perspective. For this reason, in this paper we mainly focus on the critical temperature T_C of the FM transition, instead. This quantity is absolutely independent on any specific technical issue of μ^+ SR and it is the right choice when one wants to build a robust and comprehensive general picture for the family of RCoPO materials. We show that T_C is linearly dependent both on the volume of the unit crystallographic cell and on the ionic radius of R ions over a wide experimental range. At the same time, T_C linearly depends on the external pressure as well for all the investigated compounds in a quantitatively comparable fashion. Accordingly, also supported by *ab initio* calculations, we provide a detailed and unambiguous evidence for a direct correspondence between external pressure and the lattice shrinkage induced by R ions. As such, these are demonstrated to affect the main ferromagnetic instability only via the induced structural shrinkage without involving any active role from the electronic f degrees of freedom.

II. TECHNICAL DETAILS

Loose powders of LaCoPO, PrCoPO, NdCoPO, and SmCoPO were grown via standard solid-state reactions [28] and their structural properties were investigated at ambient temperature (T) and ambient P by means of x-ray diffraction (XRD). The samples crystallized in the tetragonal phase, space group $P4/nmm$, diffraction patterns and Rietveld refinements being reported in Refs. [27] and [28]. For the aim of clarity, the lattice parameters a and c for all the materials are summarized in Table I together with the ionic radius value r_1 for the corresponding rare-earth ion R in a valence state 3+ and with a coordination number 8 (see Ref. [38]). A clear correlation of r_1 with the unit cell volume V is observed. It should be stressed that the chemical shrinkage of the cell driven by R ions is a well-known effect for the 1111 family of compounds [31,39,40].

Measurements of dc magnetometry were carried out on a commercial physical property measurement system

TABLE I. Results of Rietveld refinements of x-ray powder diffraction patterns reported in Refs. [27] and [28]. Lattice parameters a and c for the investigated compounds are reported together with the corresponding volume V of the tetragonal unit cell and the ionic radius r_1 for the R ions.

Compound	a (Å)	c (Å)	V (Å ³)	r_1 (Å)
LaCoPO	3.968(7)	8.368(3)	131.754	1.18
PrCoPO	3.921(5)	8.212(4)	126.253	1.14
NdCoPO	3.904(2)	8.182(2)	124.704	1.12
SmCoPO	3.877(4)	8.072(9)	121.331	1.09

(PPMS) and on a superconducting quantum interference device (SQUID) magnetometer magnetic property measurement system (MPMS) by Quantum Design.

μ^+ SR measurements [41,42] were performed at the $S\mu S$ muon source (Paul Scherrer Institut, Switzerland), in conditions of zero external magnetic field (ZF) and for $1.6 \text{ K} \leq T \leq 300 \text{ K}$. The GPS and Dolly spectrometers ($\pi M3$ and $\pi E1$ beam lines, respectively) were employed to perform low-background measurements at ambient pressure. These were needed as independent references for the subsequent experiments performed on the GPD spectrometer ($\mu E1$ beam line). Here, external pressures $P \leq 24 \text{ kbar}$ were applied at ambient T by means of a double-wall piston-cylinder pressure cell (PC) made of MP35N alloy, the transmitting medium Daphne oil 7373 assuring nearly hydrostatic P conditions in the whole experimental range [43]. ac susceptometry was employed in order to detect the shift of the superconducting critical temperature of a small In wire inside the PC at $T \sim 3 \text{ K}$ and to accurately quantify P in turn. μ^+ SR data analysis was performed similarly to what is discussed in Ref. [27], and the same notation will be employed in the current paper for the aim of clearness. In particular, the general expression

$$A_T(t) = A_0 \left[a_{\text{PC}} e^{-\frac{\sigma_{\text{PC}}^2 t^2}{2} - \lambda_{\text{PC}} t} + (1 - a_{\text{PC}}) G_T^s(t) \right] \quad (1)$$

was employed in order to fit the time (t) dependence of the measured spin (de)polarization $P_T \equiv A_T/A_0$ for the implanted μ^+ at all the investigated T values. Here, A_T is the so-called asymmetry function while A_0 is an experimental spectrometer-dependent parameter accounting for the maximum value of A corresponding to full spin polarization ($\sim 100 \%$). When performing experiments on the low-background GPS and Dolly spectrometers, $a_{\text{PC}} \simeq 0$ arises from the μ^+ implanted into the sample holder, into the cryostat walls, etc. At the same time, for measurements on the GPD spectrometer, $a_{\text{PC}} \simeq 0.5-0.65$ mainly accounts for the fraction of incoming μ^+ stopping in the PC. The spin polarization is here affected by the nuclear magnetism of the MP35N alloy resulting in a damping governed by the Gaussian and Lorentzian parameters σ_{PC} and λ_{PC} . The T dependence of these quantities was independently estimated in a dedicated set of measurements on the empty PC. It should be remarked that, when ferromagnetic or superconducting samples are loaded into the PC and when performing measurements in the presence of an external magnetic field, a stray field is induced outside the sample space. This leads to a complicated modulation of the local field within the PC, which can be accounted for by introducing a proper profile function and generalizing Eq. (1) accordingly [23,44].

In the case of magnetic materials, the function

$$G_T^s(t) = [1 - V_m(T)] e^{-\frac{\sigma_m^2 t^2}{2}} + [a^\perp(T) F(t) D^\perp(t) + a^\parallel(T) D^\parallel(t)] \quad (2)$$

is employed in order to describe the spin (de)polarization arising from the remaining fraction $(1 - a_{\text{PC}})$ of μ^+ , that is, the particles implanted into the sample. $V_m(T)$ is the fraction of μ^+ probing static local magnetic fields (i.e., the magnetic volume fraction of the investigated material, due to the random

implantation of μ^+). For $V_m(T) = 0$, only nuclear magnetic moments can cause a damping of the signal. Typically this damping is of Gaussian nature with characteristic rate $\sigma_N \sim 0.1 \mu\text{s}^{-1}$. Below T_C , the superscript \perp (\parallel) refers to μ^+ probing a local static magnetic field in a perpendicular (parallel) direction with respect to the initial μ^+ spin polarization and, accordingly, one has $[a^\perp(T) + a^\parallel(T)] = V_m(T)$ for the so-called transversal (a^\perp) and longitudinal (a^\parallel) fractions. A coherent precession of μ^+ around the local field B_μ generated by a LRO magnetic order can be observed in the transversal amplitude. This is typically described by the oscillating function $F(t)$, the standard choice $F(t) = \cos(\gamma B_\mu t + \phi)$ being in good agreement with current experimental data (statistical $\chi^2 \simeq 1 - 1.2$) at all T values. Here, $\gamma = 2\pi \times 135.54 \text{ MHz/T}$ is the gyromagnetic ratio for μ^+ , while typical phase values $|\phi| \sim 20^\circ - 30^\circ$ are measured (negative values are found – see also the discussion in Ref. [27]). The damping function $D^\perp(t)$ reflects a static distribution of local magnetic fields while the longitudinal component typically probes dynamical spin-lattice-like relaxation processes resulting in an exponential damping function $D^\parallel(t)$.

First-principles calculations were performed using the VASP package [45,46] within the generalized gradient approximation (GGA) to DFT [47] and projected augmented-wave (PAW) [48] pseudopotentials for both the nonmagnetic and ferromagnetic structures. Full relaxation of the cell shape and of the internal positions was achieved using 650 eV as energy cutoff and a (12, 12, 6) k -point mesh within the Monkhorst-Pack scheme [49] and making the *ab initio* forces to vanish (up to 0.001 eV/Å) at each fixed cell volume.

III. EXPERIMENTAL RESULTS

A. Summary of main results from Ref. [27] on LaCoPO and PrCoPO

In a previous work [27] we reported on a μ^+ SR investigation of magnetism in LaCoPO and PrCoPO. A LRO-

FM phase with critical temperature $T_C = 33.2 \pm 1.0 \text{ K}$ and $T_C = 48.0 \pm 1.0 \text{ K}$ develops for LaCoPO and PrCoPO, respectively. The T dependence of the local magnetic field at the μ^+ site B_μ is well described for $T \leq T_C$ by a power-law function [27]

$$B_\mu(T) = B_\mu(0) \left(1 - \frac{T}{T_C}\right)^\zeta, \quad (3)$$

where $\zeta = 0.34 \pm 0.01$ for both LaCoPO and PrCoPO. In spite of the qualitatively identical behavior, La^{3+} is a nonmagnetic ion at variance with Pr^{3+} . Accordingly, the only contribution to $B_\mu(T)$ must arise from the Co sublattice alone in both the cases and, moreover, the functional form in Eq. (3) must be intrinsically associated to the FM phase from Co. The observed behavior is qualitatively preserved independently on the actual P value, while a clear dependence on P was detected for both $B_\mu(0)$ and T_C . A detailed discussion was presented in Ref. [27] concerning the former quantity. Here, we want to mostly concentrate on T_C , which was found to linearly increase with P in both LaCoPO and PrCoPO [27].

B. NdCoPO and SmCoPO at ambient pressure

The current μ^+ SR measurements on NdCoPO and SmCoPO clearly evidence a different scenario if compared to what was reported for LaCoPO and PrCoPO. In fact, the magnetic moments of Nd^{3+} and Sm^{3+} ions crucially dominate the magnetic properties at low T and the interplay of d and f electrons leads to progressive reordering effects within the Co sublattice [28,30]. This is confirmed by our measurements of ZF- μ^+ SR and dc magnetometry both for NdCoPO and SmCoPO at ambient P .

As is shown in the insets of Fig. 1, well-defined spontaneous coherent oscillations appear in the μ^+ SR depolarization curves below $\sim 55 \text{ K}$ and $\sim 65 \text{ K}$ for NdCoPO and SmCoPO, respectively, indicating the development of a magnetic LRO phase in both the samples. These values also correspond to the sudden increase of the dc magnetization M , as is reported in the main panels of Fig. 1. Just below this transition, $B_\mu(T)$

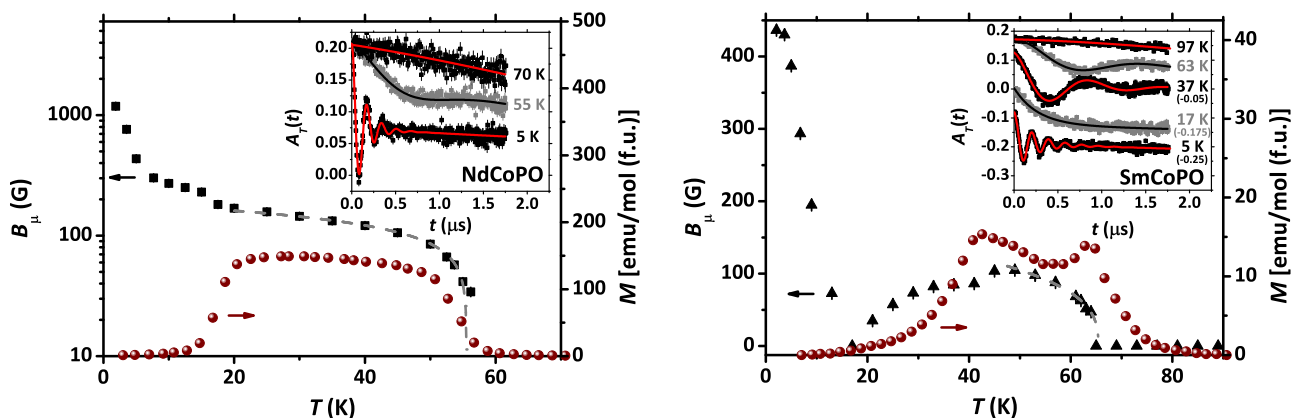


FIG. 1. (Color online) Main experimental results for NdCoPO (left) and SmCoPO (right) at ambient P : T dependence of the internal magnetic field at the μ^+ site from the low-background ZF- μ^+ SR measurements (black filled symbols) and of the field-cooled dc magnetization M at $H = 10 \text{ Oe}$ (red filled circles). M for SmCoPO is reported after the subtraction of a small linear term accounting for the contribution of magnetic extrinsic phases. For both samples, the dashed gray line is a best fit according to Eq. (3) with $\zeta = 0.34$ as fixed parameter. Insets: ZF- μ^+ SR depolarization curves at representative T values (ambient P , low-background spectrometers). Continuous lines are best-fitting curves according to Eqs. (1) and (2).

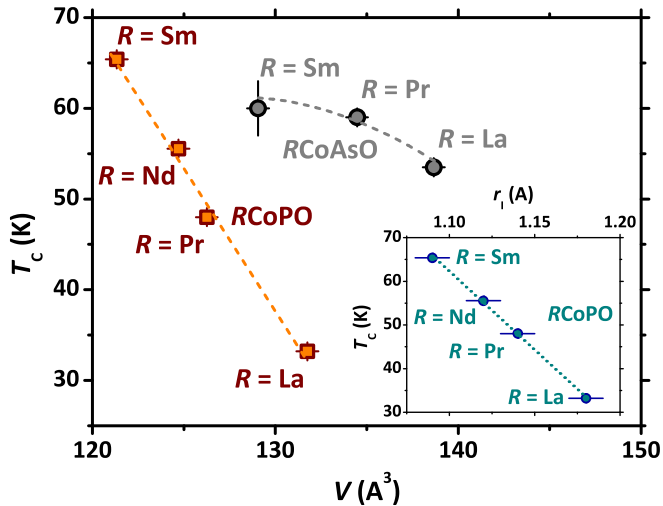


FIG. 2. (Color online) Main: dependence of T_C on the measured volume V of the tetragonal unit cell at ambient P for $R\text{CoPO}$ and for the isostructural $R\text{CoAsO}$ (these latter data are taken from Ref. [37]). The orange dashed curve is a linear best fitting to $R\text{CoPO}$ data while the gray curve is a guide to the eye. Inset: dependence of the critical temperature T_C of $R\text{CoPO}$ on the ionic radius r_1 of R ions, see Table I. The dotted curve is a linear best fitting to data.

can be well reproduced by the power-law expression reported in Eq. (3), again with $\zeta \simeq 0.34$. By assuming that $\zeta = 0.34$ (fixed parameter), a fitting of $B_\mu(T)$ data leads to the estimates $T_C = 55.5 \pm 1.0$ K and $T_C = 65.4 \pm 1.0$ K for NdCoPO and SmCoPO , respectively (see the dashed lines in the main panels of Fig. 1). However, such trend for $B_\mu(T)$ is no longer obeyed below $T_N \sim 16$ K and $T_N \sim 45$ K for NdCoPO and SmCoPO , respectively, where clear anomalies in the $M(T)$ curves are also detected. With further decreasing T below T_N , M vanishes while $B_\mu(T)$ diverges to positive values in the case of NdCoPO , while a negative divergence is rather observed for SmCoPO . In this respect, it should be explicitly recalled that $\mu^+\text{SR}$ does not measure the sign of $B_\mu(T)$, rather its absolute value. Accordingly, the cusp detected for SmCoPO at ~ 18 K should be considered as an experimental artifact arising from an undetectable sign change.

The results above can be understood as follows. As $B_\mu(T)$ for NdCoPO and SmCoPO is well reproduced by Eq. (3) with $\zeta = 0.34$ for $T_N < T < T_C$, it is reasonable to associate the magnetic transition at T_C to a FM phase originating from Co similarly to what is achieved in LaCoPO and PrCoPO . To further confirm these arguments, we report the T_C values for the four $R\text{CoPO}$ samples in the main panel of Fig. 2 as a function of the relative measured V values for the tetragonal unit cell at ambient T and P and, in the inset, as a function of the r_1 of the corresponding R ion (see Table I). Not only it is evident that the lattice shrinkage triggered by smaller ionic radii is inducing a dramatic increase of T_C (being even doubled by a full replacement of La with Sm), but a linear correlation is clearly observed between T_C and both V and r_1 . Another transition develops on the Co sublattice at T_N , with globally AFM correlations, as is indicated by the gradual vanishing of M (Fig. 1), possibly favored by the magnetic moments of the R ions. The positive and negative divergences of $B_\mu(T)$

in NdCoPO and SmCoPO , respectively, may be originating from several reasons among which, e.g., different microscopic magnetic configurations or statistical occupancies of the two μ^+ crystallographic sites in the two materials [37,50]. These issues are beyond the scope of this paper.

It should be remarked that the peculiar linear relation between structural parameters and magnetism is not at all a general feature of Co-based 1111 oxypnictides. In particular, the main panel of Fig. 2 also reports T_C vs. V data for the isostructural compounds $R\text{CoAsO}$ [37]. Here, the linear relation among these two quantities ceases as if the internal pressure effects are saturated yielding to a constant T_C when approaching the smaller size of Sm. Accordingly, no change of T_C has been observed as a function of external pressure as well in SmCoAsO [37].

C. NdCoPO and SmCoPO for nonzero external pressure

We further investigated the impact of the crystallographic structure on magnetism in NdCoPO and SmCoPO upon the increase of P . As main result (see Fig. 3), no qualitative changes are induced by P in the T dependence of B_μ whose shape is preserved identical to what is reported in Fig. 1. However, on a quantitative level, T_C is enhanced by P in a linear fashion for both NdCoPO and SmCoPO , as is evidenced in the insets of Fig. 3. Overall, the situation is extremely reminiscent of what was observed in LaCoPO and PrCoPO , where P induces a linear increase of T_C as well [27]. Similarly to those compounds and as is shown in the insets of Fig. 3, the shape of $B_\mu(T)$ is not affected at all by P just below T_C . Accordingly, Eq. (3) can still be used for $T > T_N$ as a fitting function with fixed parameter $\zeta = 0.34$ in order to estimate $T_C(P)$ (see Fig. 5 later on). At the same time, T_N is clearly suppressed upon increasing P for NdCoPO . In particular, $T_N = (16.25 \pm 1.25)$ K at ambient P shifts to $T_N = (11.7 \pm 0.7)$ K at $P = 23.8$ kbar. The simultaneous T_C enhancement and T_N suppression is reminiscent of the effect of increasing magnetic field both in NdCoPO [28] and in NdCoAsO [12]. On the other hand, T_N seems to be mostly unaffected by P for SmCoPO , however, in this case the density of experimental points does not allow us to make any definite statement.

IV. DISCUSSION

For itinerant ferromagnets, the magnetic instability is generally considered to be marked by the Stoner factor $S = I_{xc} \times D(E_F)$ becoming larger than 1. Here, I_{xc} is the exchange integral, measuring the strength of the exchange interaction sensitive to the localization of the wave functions, while $D(E_F)$ represents the density of states at the Fermi level, whose main contributions come from Co d -like components. An estimate of $D(E_F)$ is achieved on *ab initio* grounds at the experimental lattice constants of $R\text{CoPO}$ at ambient pressure, as is displayed by the red squares in the main panel of Fig. 4. Accordingly, S can be computed as well by taking a value $I_{xc} = 0.99$ for cobalt [51]. As a result, we find that the Stoner condition for FM instability is always safely satisfied for all the considered $R\text{CoPO}$ compounds. Indeed, the FM state has a lower energy than the nonmagnetic one, the total energy

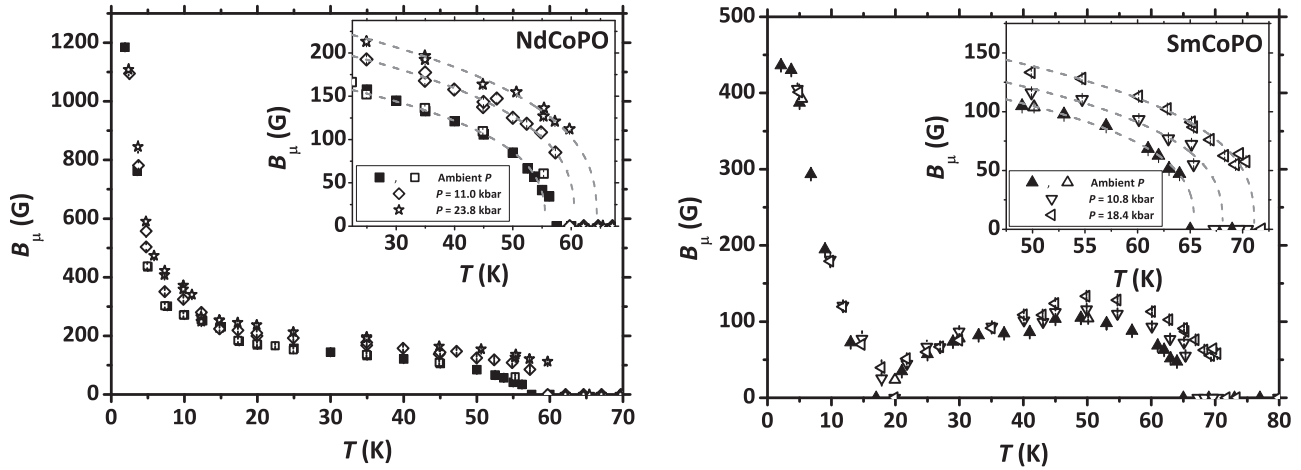


FIG. 3. T dependence of the internal field at the μ^+ site for NdCoPO (left) and SmCoPO (right) for $P < 24$ kbar (open symbols). Black filled symbols are relative to low-background measurements (reproduced from Fig. 1). Insets display an enlargement of the T region just below T_C . For both samples, the dashed gray lines are best fits according to Eq. (3) with $\zeta = 0.34$ as fixed parameter.

difference being of the order of 50–60 meV/cell for every compound. According to some theoretical models [52,53], $D(E_F)$ is expected to be directly related to T_C and, although the increase of $D(E_F)$ discussed above will surely result in a positive contribution to T_C , we find from calculations that the small actual variation in its absolute value with chemical or external pressures can not explain the large differences reported in the main panel of Fig. 2. Moreover, the qualitative discrepancies between $R\text{CoAsO}$ and $R\text{CoPO}$ presented in Fig. 2 also imply a nontrivial difference in the microscopic

origin of the link between structure and magnetism. This may likely involve different degrees of hybridization between the pnictogen and the transition metal and quantitatively different exchange paths.

The green diamonds in the main panel of Fig. 4 are $D(E_F)$ values calculated for LaCoPO under external pressure and, remarkably, these values very closely mimic the trend of the different compounds at their respective equilibrium volumes, showing that the main variation is essentially linked to the internal pressure effect induced by the smaller R . This provides additional evidence that the change in the electronic properties of $R\text{CoPO}$ is merely due to structure and that the f states associated with the R ions do play a likely passive role.

The equilibrium structural parameters a_{calc} and c_{calc} in the ferromagnetic state are further results of our *ab initio* calculations and are reported in Table II together with their experimental counterparts (see Table I). As can be observed, both the experimental trends of a and c and their fractional changes are reproduced with high accuracy by our calculations. As is shown in the inset of Fig. 4, the corresponding calculated equilibrium volumes V_{calc} for all the considered compounds reproduce very nicely the experimental trend of V (see the dashed line in the inset). This is true both qualitatively and quantitatively within the usual DFT-GGA accuracy. The calculated magnetic moment of Co atoms decreases with reducing the volume of the tetragonal cell from $0.52 \mu_B$ in LaCoPO to $0.48 \mu_B$ for SmCoPO. While this trend is in qualitative agreement with the experimental results of dc

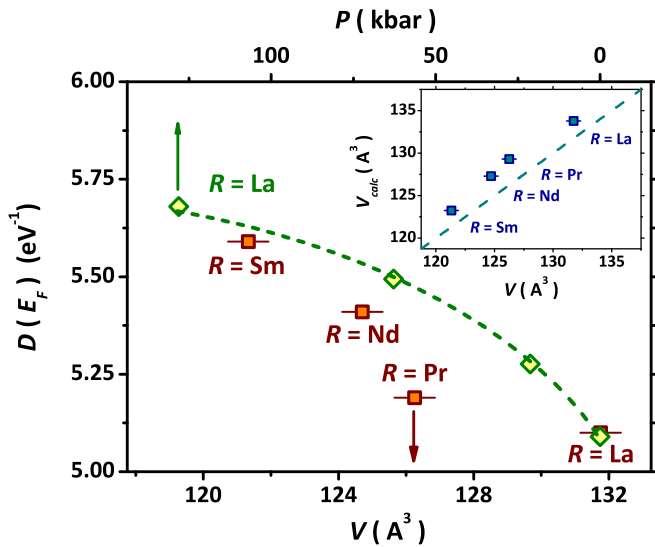


FIG. 4. (Color online) Main: density of states at the Fermi level $D(E_F)$ for the investigated $R\text{CoPO}$ compounds as a function of the experimental value of the unit cell volume V (open squares, relative to lower x axis). The $D(E_F)$ values calculated for the LaCoPO compound are also reported at different volumes corresponding to pressure values indicated on the upper x axis (open diamonds). The dashed line is a guide to the eye. Inset: dependence of the calculated unit cell volume in the FM state V_{calc} on the experimental V for the four investigated $R\text{CoPO}$ compounds at ambient P . The dashed line represents the condition $V_{\text{calc}} = V$.

TABLE II. Comparison of the experimental structural parameters a and c (see Table I) and the calculated equilibrium corresponding quantities a_{calc} and c_{calc} .

Compound	a (Å)	a_{calc} (Å)	c (Å)	c_{calc} (Å)
LaCoPO	3.968(7)	3.969	8.368(3)	8.503
PrCoPO	3.921(5)	3.947	8.212(4)	8.342
NdCoPO	3.904(2)	3.921	8.182(2)	8.226
SmCoPO	3.877(4)	3.886	8.072(9)	8.146

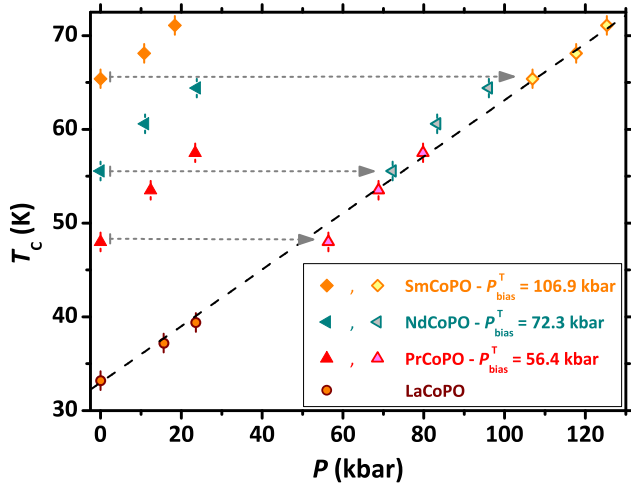


FIG. 5. (Color online) Summarizing results of T_C vs. P for the four investigated $R\text{CoPO}$ samples (full symbols). The slope of the dashed line is obtained by Eq. (4), see text. Data for PrCoPO, NdCoPO and SmCoPO are also shifted horizontally (open symbols) by the calculated sample-specific amounts P_{bias}^T mimicking the effect of chemical pressure (see the discussion in the text).

magnetometry for LaCoPO and PrCoPO [27], the strong magnetic contribution from R ions makes an experimental check uncertain for both NdCoPO and SmCoPO.

The experimental results for the actual dependence of T_C on P in $R\text{CoPO}$ are summarized in Fig. 5. It is apparent that pressure leads to a linear enhancement of T_C with a quantitatively similar slope for all the considered $R\text{CoPO}$ compounds. By considering the observations above (Fig. 2) concerning the linear dependence of T_C on V at ambient pressure, it is possible to discuss the close correspondence between chemical and external pressures more in detail. In particular, it is straightforward to speculate that external pressure linearly influences V , which, in turn, linearly enhances T_C .

These arguments can be substantiated by computing the isothermal lattice compressibility $\beta = -(1/V) \times (dV/dP)$ for LaCoPO by means of first-principles calculations. The obtained values are $7.52 \times 10^{-4} \text{ kbar}^{-1}$ and $7.23 \times 10^{-4} \text{ kbar}^{-1}$ in the paramagnetic and FM states, respectively. The assumption about the linear influence of both chemical and external pressures on V can now be exploited by writing

$$\beta = -\frac{1}{V} \frac{dV}{dP} = -\frac{1}{V} \frac{\partial V}{\partial T_C} \frac{\partial T_C}{\partial P}. \quad (4)$$

Inverting Eq. (4) and using the experimental estimate of $\partial V/\partial T_C$ from Fig. 2, an estimate can be given for the partial derivative $\partial T_C/\partial P$ (the normalization factor $1/V$ is obtained from the ambient P value $V = 131.754 \text{ \AA}^3$). This method is necessarily approximate, as V values at room T are involved together with T_C , whose values are ~ 1 order of magnitude smaller. However, this uncertainty can be approximately solved in Eq. (4) by selecting an intermediate value for the computed compressibility, namely $\beta \simeq 7.4 \times 10^{-4} \text{ kbar}^{-1}$. This is admissible also in view of the tiny discrepancy ($\sim 4\%$) among the two β values reported above.

A line with slope given by the calculated $\partial T_C/\partial P$ is then reported in Fig. 5. In order to better compare the $T_C(P)$

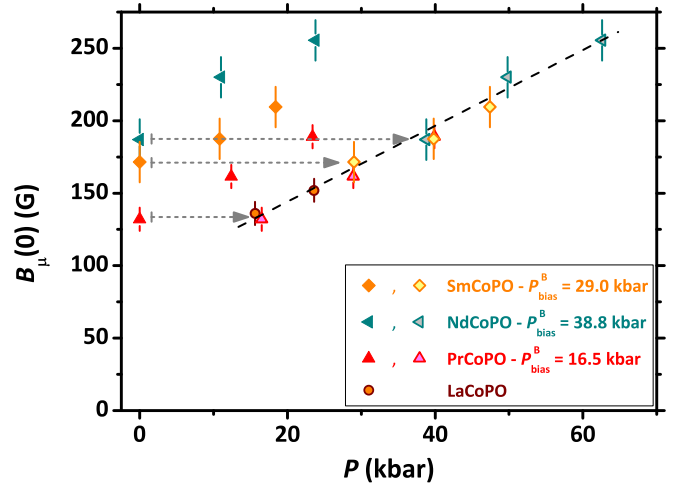


FIG. 6. (Color online) Zero-temperature extrapolations of B_μ for the four samples and at the different investigated P values (full symbols). Data for LaCoPO and PrCoPO are reproduced from Ref. [27]. Data for PrCoPO, NdCoPO and SmCoPO are also shifted horizontally (open symbols) by the empirical sample-specific amounts P_{bias}^B mimicking the effect of chemical pressure (see the discussion in the text). The dashed line is a guide to the eye.

experimental data to the computed line, we consider the effect of chemical pressure introduced by R ions as mimicked by a constant P_{bias}^T offsets characteristic of each sample. These can be easily calculated from first-principles calculations as the pressure values needed to make LaCoPO volume match exactly the $R\text{CoPO}$ equilibrium volumes (for $R = \text{Pr, Nd, and Sm}$) and are reported in Fig. 5. When the experimental data points are shifted by the corresponding P_{bias}^T amounts, they all collapse on the line calculated by Eq. (4), as is shown in Fig. 5. This linear correlation of experimental points in excellent agreement with the calculated line strongly supports the picture that R ions act as an effective external isotropic pressure and is a compelling indication towards the full equivalence of chemical and external pressures.

Finally, we consider the effect of pressure on the internal magnetic field B_μ at the μ^+ site. In our previous work [27], we presented the P dependence of the B_μ experimental values at $T = 5 \text{ K}$ and by shifting data of PrCoPO by a constant empirical offset P_{bias}^B . Here we follow the same approach but we rather consider the zero-temperature extrapolations $B_\mu(0)$ for the four compounds at the different P values, the reason being the low- T magnetic contributions from Nd^{3+} and Sm^{3+} ions in NdCoPO and SmCoPO (see Figs. 1 and 3). This leads to a larger experimental error for these two compounds due to the smaller high-temperature fitting regions. In Fig. 6 we report the results for the four samples and, at the same time, we report the data for PrCoPO, NdCoPO and SmCoPO after shifting them by empirical sample-dependent quantities P_{bias}^B (their values are reported in the graph). As is mentioned in the introduction, B_μ is a rather delicate quantity in the comparison between different samples, as the implantation sites may be nonequivalent even for isostructural compounds [37,50] and, accordingly, a quantitative analysis could be easily misleading. For this reason, it is not expected *a priori* that the biasing pressures obtained for $T_C(P)$ in Fig. 5 should be equal to

the ones currently obtained for $B_\mu(0)$. Stated otherwise, it is not expected that $P_{\text{bias}}^T = P_{\text{bias}}^B$, which is indeed not the case experimentally after comparing Fig. 5 and Fig. 6. Still, the framework discussed above is qualitatively preserved, namely – within the experimental uncertainty – a linear behavior with a common slope for the four compounds is reported for the internal field as well. This evidence further supports the full equivalence between chemical and external pressures in $R\text{CoPO}$.

V. CONCLUSIONS

In this paper, we have extended our previous $\mu^+\text{SR}$ investigation of itinerant ferromagnetism in LaCoPO and PrCoPO to the cases of NdCoPO and SmCoPO . The magnetic moment arising from electronic f shells and localized on the Nd^{3+} and Sm^{3+} ions plays a key role in the overall magnetic properties of the compounds at low temperatures. However, as long as only the ferromagnetic phase at higher temperatures is considered, a strong correlation of the magnetic and structural properties is reported and discussed. The critical temperature T_C proper of the ferromagnetic phase is linearly dependent on the volume of the unit crystallographic cell and on the ionic radius of R ions over a wide experimental range. Its value can be even doubled by a full replacement of La with Sm. At the same time, T_C linearly depends on the external pressure as well for all the investigated compounds in a quantitatively comparable fashion. Accordingly, also supported by *ab initio* calculations, we provide a detailed and unambiguous evidence

for a direct correspondence between the structural shrinkage induced by external and chemical pressures. As such, the ferromagnetic instability is driven in these compounds only by the crystallographic structure without involving any active role from the electronic f degrees of freedom. Calculations based on the variation in the density of states at the Fermi energy upon increasing pressures are not able to quantitatively reproduce the full enhancement T_C , opening the way to further theoretical investigations of these materials. In this respect, we recall that two-dimensional–three-dimensional crossover for spin-fluctuations have been put forward to explain previous experimental results [30,31] and that a first-principles finite-temperature description of itinerant ferromagnets remains a big challenge in condensed matter theory.

ACKNOWLEDGMENTS

We acknowledge useful discussions with C. Ortix, R. De Renzi, and P. Carretta. G.P. acknowledges support by the Humboldt Research Fellowship for Postdoctoral researchers. S.S. acknowledges partial support of PRIN2012 Project No. 2012X3YFZ2. A.P. acknowledges financial support from the Dr. D. S. Kothari Postdoctoral Fellowship (UGC-DSKPDF) Program. This research at NPL, New Delhi, is supported by the DAE-SRC outstanding Investigator Award Scheme. The experimental $\mu^+\text{SR}$ work was performed at the Swiss Muon Source ($S\mu S$) at the Paul Scherrer Institut, Switzerland.

-
- [1] G. Xu, W. Ming, Y. Yao, X. Dai, S.-C. Zhang, and Z. Fang, Doping-dependent phase diagram of LaOMAs ($M = \text{V} - \text{Cu}$) and electron-type superconductivity near ferromagnetic instability, *Europhys. Lett.* **82**, 67002 (2008).
- [2] Y. Kamihara, T. Watanabe, M. Hirano, and H. Hosono, Iron-based layered superconductor $\text{La}[\text{O}_{1-x}\text{F}_x]\text{FeAs}$ ($x = 0.05 - 0.12$) with $T_c = 26$ K, *J. Am. Chem. Soc.* **130**, 3296 (2008).
- [3] Z.-A. Ren, W. Lu, J. Yang, W. Yi, X.-L. Shen, Z.-C. Li, G.-C. Che, X.-L. Dong, L.-L. Sun, F. Zhou, and Z.-X. Zhao, Superconductivity at 55 K in Iron-based F-doped layered quaternary compound $\text{Sm}[\text{O}_{1-x}\text{F}_x]\text{FeAs}$, *Chin. Phys. Lett.* **25**, 2215 (2008).
- [4] D. C. Johnston, The puzzle of high temperature superconductivity in layered iron pnictides and chalcogenides, *Adv. Phys.* **59**, 803 (2010).
- [5] G. R. Stewart, Superconductivity in iron compounds, *Rev. Mod. Phys.* **83**, 1589 (2011).
- [6] G. Prando, A. Lascialfari, A. Rigamonti, L. Romanò, S. Sanna, M. Putti, and M. Tropeano, Superconducting phase fluctuations in $\text{SmFeAsO}_{0.8}\text{F}_{0.2}$ from diamagnetism at a low magnetic field above T_c , *Phys. Rev. B* **84**, 064507 (2011).
- [7] C. Krellner, N. S. Kini, E. M. Brüning, K. Koch, H. Rosner, M. Nicklas, M. Baenitz, and C. Geibel, CeRuPO : A rare example of a ferromagnetic Kondo lattice, *Phys. Rev. B* **76**, 104418 (2007).
- [8] H. Kotegawa, T. Toyama, S. Kitagawa, H. Tou, R. Yamauchi, E. Matsuoka, and H. Sugawara, Pressure-temperature-magnetic field phase diagram of ferromagnetic kondo lattice CeRuPO , *J. Phys. Soc. Jpn.* **82**, 123711 (2013).
- [9] H. Yanagi, R. Kawamura, T. Kamiya, Y. Kamihara, M. Hirano, T. Nakamura, H. Osawa, and H. Hosono, Itinerant ferromagnetism in the layered crystals LaCoOX ($X=\text{P,As}$), *Phys. Rev. B* **77**, 224431 (2008).
- [10] N. Emery, E. J. Wildman, J. M. S. Skakle, G. Giriat, R. I. Smith, and A. C. Mclaughlin, Giant magnetoresistance in oxypnictides (La,Nd)OMnAs, *Chem. Commun.* **46**, 6777 (2010).
- [11] N. Emery, E. J. Wildman, J. M. S. Skakle, A. C. Mclaughlin, R. I. Smith, and A. N. Fitch, Variable temperature study of the crystal and magnetic structures of the giant magnetoresistant materials LMnAsO ($L = \text{La, Nd}$), *Phys. Rev. B* **83**, 144429 (2011).
- [12] H. Ohta, C. Michioka, and K. Yoshimura, Large magnetoresistance effects in LnCoAsO ($\text{Ln} = \text{Nd, Sm}$) with a ferromagnetic-antiferromagnetic transition, *Phys. Rev. B* **84**, 134411 (2011).
- [13] A. Pal, M. Tropeano, S. D. Kaushik, M. Hussain, H. Kishan, and V. P. S. Awana, Intriguing complex magnetism of Co in RECoAsO ($\text{RE} = \text{La, Nd, and Sm}$), *J. Appl. Phys.* **109**, 07E121 (2011).
- [14] Y. Shiomi, S. Ishiwata, Y. Taguchi, and Y. Tokura, Mott insulator to metal transition in filling-controlled SmMnAsO_{1-x} , *Phys. Rev. B* **84**, 054519 (2011).
- [15] E. J. Wildman, J. M. S. Skakle, N. Emery, and A. C. Mclaughlin, Colossal magnetoresistance in Mn^{2+} oxypnictides $\text{NdMnAsO}_{1-x}\text{F}_x$, *J. Am. Chem. Soc.* **134**, 8766 (2012).

- [16] D. J. Singh and M.-H. Du, Density Functional Study of $\text{LaFeAsO}_{1-x}\text{F}_x$: A Low Carrier Density Superconductor Near Itinerant Magnetism, *Phys. Rev. Lett.* **100**, 237003 (2008).
- [17] S. Graser, T. A. Maier, P. J. Hirschfeld, and D. J. Scalapino, Near-degeneracy of several pairing channels in multiorbital models for the Fe pnictides, *New J. Phys.* **11**, 025016 (2009).
- [18] M. M. Qazilbash, J. J. Hamlin, R. E. Baumbach, L. Zhang, D. J. Singh, M. B. Maple, and D. N. Basov, Electronic correlations in the iron pnictides, *Nature Phys.* **5**, 647 (2009).
- [19] L. De' Medici, *Weak and Strong Correlations in Fe Superconductors*, Springer Series in Materials Science Vol. 211, p. 409 (Springer, Berlin, 2015).
- [20] G. Prando, P. Carretta, A. Rigamonti, S. Sanna, A. Palenzona, M. Putti, and M. Tropeano, ^{19}F NMR study of the coupling between $4f$ and itinerant electrons in the pnictide superconductors $\text{SmFeAsO}_{1-x}\text{F}_x$ ($0.15 \leq x \leq 0.2$), *Phys. Rev. B* **81**, 100508(R) (2010).
- [21] G. Prando, S. Sanna, G. Lamura, T. Shiroka, M. Tropeano, A. Palenzona, H.-J. Grafe, B. Büchner, P. Carretta, and R. De Renzi, Phase separation at the magnetic-superconducting transition in $\text{La}_{0.7}\text{Y}_{0.3}\text{FeAsO}_{1-x}\text{F}_x$, *Phys. Stat. Sol. B* **250**, 599 (2013).
- [22] K. Miyoshi, E. Kojima, S. Ogawa, Y. Shimojo, and J. Takeuchi, Superconductivity under pressure in $R\text{FeAsO}_{1-x}\text{F}_x$ ($R = \text{La, Ce-Sm}$) by dc magnetization measurements, *Phys. Rev. B* **87**, 235111 (2013).
- [23] G. Prando, Th. Hartmann, W. Schottenhamel, Z. Guguchia, S. Sanna, F. Ahn, I. Nekrasov, C. G. F. Blum, A. U. B. Wolter, S. Wurmehl, R. Khasanov, I. Eremin, and B. Büchner, Mutual Independence of Critical Temperature and Superfluid Density under Pressure in Optimally Electron-Doped Superconducting $\text{LaFeAsO}_{1-x}\text{F}_x$, *Phys. Rev. Lett.* **114**, 247004 (2015).
- [24] G. Prando, O. Vakaliuk, S. Sanna, G. Lamura, T. Shiroka, P. Bonfà, P. Carretta, R. De Renzi, H.-H. Klauss, C. G. F. Blum, S. Wurmehl, C. Hess, and B. Büchner, Role of in-plane and out-of-plane dilution in CeFeAsO : Charge doping versus disorder, *Phys. Rev. B* **87**, 174519 (2013).
- [25] N. Qureshi, Y. Drees, J. Werner, S. Wurmehl, C. Hess, R. Klingeler, B. Büchner, M. T. Fernández-Díaz, and M. Braden, Crystal and magnetic structure of the oxypnictide superconductor $\text{LaFeAsO}_{1-x}\text{F}_x$: A neutron-diffraction study, *Phys. Rev. B* **82**, 184521 (2010).
- [26] R. De Renzi, P. Bonfà, M. Mazzani, S. Sanna, G. Prando, P. Carretta, R. Khasanov, A. Amato, H. Luetkens, M. Bendele, F. Bernardini, S. Massidda, A. Palenzona, M. Tropeano, and M. Vignolo, Effect of external pressure on the magnetic properties of LnFeAsO ($\text{Ln} = \text{La, Ce, Pr, Sm}$), *Supercond. Sci. Technol.* **25**, 084009 (2012).
- [27] G. Prando, P. Bonfà, G. Profeta, R. Khasanov, F. Bernardini, M. Mazzani, E. M. Brüning, A. Pal, V. P. S. Awana, H.-J. Grafe, B. Büchner, R. De Renzi, P. Carretta, and S. Sanna, Common effect of chemical and external pressures on the magnetic properties of RCoPO ($R = \text{La, Pr}$), *Phys. Rev. B* **87**, 064401 (2013).
- [28] A. Pal, S. S. Mehdi, M. Husain, B. Gahtori, and V. P. S. Awana, Complex magnetism and magneto-transport of RECoPO ($\text{RE} = \text{La, Nd, and Sm}$), *J. Appl. Phys.* **110**, 103913 (2011).
- [29] M. Majumder, K. Ghoshray, A. Ghoshray, A. Pal, and V. P. S. Awana, Anisotropic spin-fluctuations in SmCoPO revealed by ^{31}P NMR measurement, *J. Phys. Soc. Jpn.* **81**, 054702 (2012).
- [30] M. Majumder, K. Ghoshray, A. Ghoshray, A. Pal, and V. P. S. Awana, Local electromagnetic properties of magnetic pnictides: A comparative study probed by NMR measurements, *J. Phys.: Cond. Mat.* **25**, 196002 (2013).
- [31] H. Ohta and K. Yoshimura, Magnetic properties of LCoAsO ($L = \text{La-Gd}$), *Phys. Rev. B* **80**, 184409 (2009).
- [32] V. P. S. Awana, I. Nowik, A. Pal, K. Yamaura, E. Takayama-Muromachi, and I. Felner, Magnetic phase transitions in SmCoAsO , *Phys. Rev. B* **81**, 212501 (2010).
- [33] M. A. McGuire, D. J. Gout, V. O. Garlea, A. S. Sefat, B. C. Sales, and D. Mandrus, Magnetic phase transitions in NdCoAsO , *Phys. Rev. B* **81**, 104405 (2010).
- [34] H. Ohta, C. Michioka, A. Matsuo, K. Kindo, and K. Yoshimura, Magnetic study of SmCoAsO showing a ferromagnetic-antiferromagnetic transition, *Phys. Rev. B* **82**, 054421 (2010).
- [35] A. Marcinkova, D. A. M. Grist, I. Margiolaki, T. C. Hansen, S. Margadonna, and Jan-Willem G. Bos, Superconductivity in $\text{NdFe}_{1-x}\text{Co}_x\text{AsO}$ ($0.05 < x < 0.20$) and rare-earth magnetic ordering in NdCoAsO , *Phys. Rev. B* **81**, 064511 (2010).
- [36] J. Sugiyama, M. Mansson, O. Ofer, K. Kamazawa, M. Harada, D. Andreica, A. Amato, J. H. Brewer, E. J. Ansaldo, H. Ohta, C. Michioka, and K. Yoshimura, Successive magnetic transitions and static magnetic order in RCoAsO ($R = \text{La, Ce, Pr, Nd, Sm, Gd}$) confirmed by muon-spin rotation and relaxation, *Phys. Rev. B* **84**, 184421 (2011).
- [37] G. Prando, S. Sanna, R. Khasanov, A. Pal, E. M. Brüning, M. Mazzani, V. P. S. Awana, B. Büchner, and R. De Renzi, Effect of external pressure on the magnetic properties of RCoAsO ($R = \text{La, Pr, Sm}$): A μSR study, *J. Phys. Chem. Sol.* **84**, 63 (2015).
- [38] *CRC Handbook of Chemistry and Physics*, 89th ed., edited by D. R. Lide (CRC Press, Boca Raton, 2009), pp. 4–132.
- [39] Y. Luo, Y. Li, S. Jiang, J. Dai, G. Cao, and Z.-A. Xu, Phase diagram of $\text{CeFeAs}_{1-x}\text{P}_x\text{O}$ obtained from electrical resistivity, magnetization, and specific heat measurements, *Phys. Rev. B* **81**, 134422 (2010).
- [40] F. Nitsche, A. Jesche, E. Hieckmann, T. Doert, and M. Ruck, Structural trends from a consistent set of single-crystal data of RFeAsO ($R = \text{La, Ce, Pr, Nd, Sm, Gd, and Tb}$), *Phys. Rev. B* **82**, 134514 (2010).
- [41] S. J. Blundell, Spin-polarized muons in condensed matter physics, *Contemp. Phys.* **40**, 175 (1999).
- [42] A. Yaouanc, P. Dalmas de Réotier, *Muon Spin Rotation, Relaxation, and Resonance: Applications to Condensed Matter* (Oxford University Press, Oxford, 2011).
- [43] W. J. Duncan, O. P. Welzel, C. Harrison, X. F. Wang, X. H. Chen, F. M. Grosche, and P. G. Niklowitz, High pressure study of BaFe_2As_2 —the role of hydrostaticity and uniaxial stress, *J. Phys.: Cond. Mat.* **22**, 052201 (2010).
- [44] A. Maisuradze, A. Shengelaya, A. Amato, E. Pomjakushina, and H. Keller, Muon spin rotation investigation of the pressure effect on the magnetic penetration depth in $\text{YBa}_2\text{Cu}_3\text{O}_x$, *Phys. Rev. B* **84**, 184523 (2011).
- [45] G. Kresse and J. Furthmüller, Efficient iterative schemes for *ab initio* total-energy calculations using a plane-wave basis set, *Phys. Rev. B* **54**, 11169 (1996).
- [46] G. Kresse and J. Furthmüller, Efficiency of *ab-initio* total energy calculations for metals and semiconductors using a plane-wave basis set, *Comput. Mater. Sci.* **6**, 15 (1996).
- [47] J. P. Perdew, K. Burke, and M. Ernzerhof, Generalized Gradient Approximation Made Simple, *Phys. Rev. Lett.* **77**, 3865 (1996).

- [48] P. E. Blöchl, Projector augmented-wave method, *Phys. Rev. B* **50**, 17953 (1994).
- [49] H. J. Monkhorst and J. D. Pack, Special points for Brillouin-zone integrations, *Phys. Rev. B* **13**, 5188 (1976).
- [50] P. Bonfà, F. Sartori, and R. De Renzi, Efficient and reliable strategy for identifying muon sites based on the double adiabatic approximation, *J. Phys. Chem. C* **119**, 4278 (2015).
- [51] J. F. Janak, Uniform susceptibilities of metallic elements, *Phys. Rev. B* **16**, 255 (1977).
- [52] P. Mohn and E. P. Wohlfarth, The Curie temperature of the ferromagnetic transition metals and their compounds, *J. Phys. F: Met. Phys.* **17**, 2421 (1987).
- [53] A. B. Kaiser, A. M. Oles, and G. Stollhoff, Volume dependence of the Stoner parameter in transition metals, *Phys. Scr.* **37**, 935 (1988).